

Magnetic structure of small Fe, Mn, and Cr clusters supported on Cu(111): Noncollinear first-principles calculations

Anders Bergman,^{1,*} Lars Nordström,¹ Angela Burlamaqui Klautau,² Sonia Frota-Pessôa,³ and Olle Eriksson^{1,†}

¹*Department of Physics, Uppsala University, Box 530 Sweden*

²*Departamento de Física, Universidade Federal do Pará, Belém, PA, Brazil*

³*Instituto de Física, Universidade de São Paulo, CP 66318, São Paulo, SP, Brazil*

(Dated: March 9, 2019)

The magnetic structures of small clusters of Fe, Mn, and Cr supported on a Cu(111) surface have been studied with non-collinear first principles theory. Different geometries such as triangles, pyramids and wires are considered and the cluster sizes have been varied between two to ten atoms. The calculations have been performed using a real space linear muffin-tin orbital method (RS-LMTO-ASA). The Fe clusters are found to order ferromagnetically regardless of the cluster geometry. For Mn and Cr clusters, antiferromagnetic exchange interactions between nearest-neighbours are found to cause collinear antiferromagnetic ordering when the geometry allows it. If the antiferromagnetism is frustrated by the cluster geometry non-collinear ordering is found. A comparison between the calculated structures and ground states obtained from simplified Heisenberg Hamiltonians show that the exchange interaction varies for different atoms in the clusters as a result of the different local structure.

PACS numbers: 75.75.+a, 73.22.-f, 75.10.-b

I. INTRODUCTION

The remarkable progress of experimental methodologies with atomic resolution, such as the scanning electron microscopy¹ (STM), has paved the way for studies of nanoscale magnetic materials such as ad-atoms, clusters and wires deposited on surfaces. As a result of the reduced dimensions and symmetries for such systems, magnetic behaviour that differs from bulk materials can be found^{2,3}. This attracts interest not only for the novel physics that can occur in these systems but also for the possibility to tailor the electronic and magnetic properties by changing the structure and the local environment of the systems.

Studies of systems consisting of only a few atoms can give valuable information on how the magnetic structure evolves from single atoms towards the bulk behaviour. Fe, Mn, and Cr are all known to exhibit interesting magnetic behaviour. While being ferromagnetic in the bcc phase, Fe in the fcc phase has been found to exhibit a spin-spiral structure when synthesized as precipitates in a Cu matrix⁴ and calculations show that the magnetic structure is strongly dependent on the lattice parameter⁵. Cr has in bulk an incommensurate antiferromagnetic spin density wave⁶ which can be tuned by creating superlattices with ferromagnetic or paramagnetic layers and varying the interface roughness and layer thickness⁷. When deposited on stepped surfaces, Cr can be found to have non-collinear ordering⁸. Bulk Mn exhibits perhaps the most intriguing magnetic structure of all elements with a unit cell containing 58 atoms⁹ with a complex non-collinear antiferromagnetic magnetic structure.¹⁰ Recently, several Mn based compounds, where the magnetic ordering is non-collinear due to geometric frustration between the magnetic moments of Mn atoms, have been studied^{11,12} experimentally as

well as theoretically.

Free clusters of Fe, Mn, and Cr have been studied both experimentally and theoretically. Stern-Gerlach measurements on Fe¹³ clusters show ferromagnetic behaviour while Mn clusters¹⁴ and Cr clusters¹⁵ show varying small net deflections, which can be interpreted as the result of antiferromagnetic or even non-collinear magnetic configurations. Calculations have shown that small Mn and Cr clusters can exhibit non-collinear magnetic ordering^{16,17,18} in agreement with the Stern-Gerlach experiments.

Supported transition metal clusters have also been studied extensively where a majority of the studies have been theoretical. Among the experimental studies, most work has been done on Fe, where Fe clusters deposited on a Ni surface have been found to be ferromagnetic with oscillating magnitude of the orbital moments¹⁹ and Fe clusters supported on a graphite surface have been found to exhibit enhanced spin and orbital moments compared to bulk²⁰. Among the theoretical studies, the reported calculations have mostly only considered collinear magnetization densities. Monoatomic wires of Fe on Cu(111) and Cu(001) show ferromagnetic behaviour with a strong magnetic anisotropy^{21,22}. Small Mn clusters on Ag(001) have been found to exhibit magnetic bi-stability^{23,24} which is also the case for mixed clusters of FeMn and FeCr that have been found to have both ferro- and antiferromagnetic solutions close in energy²⁵. Early model calculations of supported equilateral triangular transition metal clusters have shown that non-collinear ordering can be obtained from the frustration due to antiferromagnetic interactions between the cluster atoms.^{26,27} Recent studies have found that small clusters of Mn and Cr become non-collinear when deposited on Ni(001)²⁸ and Fe(001)^{29,30} surfaces due to competing exchange interactions between the cluster atoms and the surface²⁸.

In a previous paper³¹ we reported on non-collinear magnetic ordering for a selection of small Mn clusters supported on a Cu surface. In this paper we expand these results and present theoretical results concerning the magnetic ordering and interactions for Fe, Mn, and Cr clusters deposited on a Cu(111) surface. The calculations have been performed using the RS-LMTO-ASA method that is a first principles order-N method which has recently been extended to the treatment of non-collinear magnetism³¹.

II. METHOD

The RS-LMTO-ASA method is based on the LMTO-ASA technique³² and the Haydock recursion method³³. The LMTO-ASA formalism provides an efficient, parameter-free, basis set for treating close packed metallic systems and the recursion method gives the ability to treat problems where translational symmetry is absent and does also convey order-N scaling with respect to the number of nonequivalent atoms in the system. The recursion method does not directly solve the eigenvalue problem as formulated in the DFT, but allows one to calculate the local density of states (LDOS) for the orbitals of the atoms in the selected system. The RS-LMTO-ASA method has successfully been used for a wide range of problems including bulk systems, multilayers, embedded impurities and clusters and clusters on surfaces. Earlier and more detailed descriptions of the collinear implementation of the RS-LMTO-ASA can be found elsewhere^{34,35}.

In the local spin density approximation (LSDA)³⁶, the electron density is expressed through a 2x2 density matrix ρ which can be expressed in terms of the non-magnetic charge density n and the magnetization density \mathbf{m} as $\rho = (n\mathcal{I} + \mathbf{m} \cdot \boldsymbol{\sigma})/2$ where \mathcal{I} is the 2x2 identity matrix and $\boldsymbol{\sigma} = \{\sigma_x, \sigma_y, \sigma_z\}$ are the Pauli matrices. Self-consistent methods^{37,38,39} for calculating the electronic structure for non-collinear magnetization densities have existed for quite some time⁴⁰, and here we will focus on the specific details for treating non-collinear magnetization densities within the RS-LMTO-ASA.

With the recursion method, the local density of states $N(\epsilon)$ where ϵ is the energy, is obtained as $N(\epsilon) = -\frac{1}{\pi} \Im \text{tr} \mathcal{G}(\epsilon)$. Here $\mathcal{G}(\epsilon)$ is the local Green's function $\mathcal{G}(\epsilon) = (\epsilon - \mathcal{H})^{-1}$, where \mathcal{H} is the Hamiltonian. Similar to the LDOS, the collinear magnetic density of states $m(\epsilon)$ can be calculated as $m(\epsilon) = -\frac{1}{\pi} \Im \text{tr}(\sigma_z \mathcal{G}(\epsilon))$. Since the Pauli spin matrix σ_z is diagonal in spin-space, the collinear magnetic density of states can be calculated using only diagonal elements of the Green's function. If a generalized non-collinear magnetization density

$$\mathbf{m}(\epsilon) = -\frac{1}{\pi} \Im \text{tr}(\boldsymbol{\sigma} \mathcal{G}(\epsilon)) \quad (1)$$

where $\boldsymbol{\sigma} = \{\sigma_x, \sigma_y, \sigma_z\}$ is sought, evaluation of the off-diagonal parts of the Green's function is in princi-

ple needed. The off-diagonal elements of the Green's function are possible to obtain by performing the recursion starting from carefully selected linear combinations of muffin-tin orbitals⁴¹ or perform a computationally more demanding block recursion calculation⁴². However, in our implementation we avoid the evaluation of off-diagonal elements by applying successive unitary transformations \mathcal{U} on the Hamiltonian, $\mathcal{H}' = \mathcal{U}\mathcal{H}\mathcal{U}^\dagger$. When the Hamiltonian is transformed in this way, the Green's function transform similarly; $\mathcal{G}' = \mathcal{U}\mathcal{G}\mathcal{U}^\dagger$.

Using the unitary property $\mathcal{U}^\dagger\mathcal{U} = 1$ and the fact that cyclic permutations of matrix multiplications conserve the trace of the product, the generalized magnetic density of states $\mathbf{m}(\epsilon)$, can be written as

$$\mathbf{m}(\epsilon) = -\frac{1}{\pi} \Im \text{tr}\{\boldsymbol{\sigma}\mathcal{U}^\dagger\mathcal{U}\mathcal{G}\mathcal{U}^\dagger\mathcal{U}\} = -\frac{1}{\pi} \Im \text{tr}\{\boldsymbol{\sigma}'\mathcal{G}'\}, \quad (2)$$

where $\boldsymbol{\sigma}'$ is the Pauli matrices after the unitary transformation. The transformation matrix \mathcal{U} is different for the three directions, and chosen so that, $\mathcal{U}\sigma_j\mathcal{U}^\dagger = \sigma'_z$, for $j = x, y, z$, to yield a diagonal representation. In the trivial case of $j = z$ the unitary transformation is just the identity matrix. For the other directions, the unitary transformation corresponds to a spin rotation where \mathcal{U} can be calculated using spin- $\frac{1}{2}$ rotation matrices. Decomposing the Hamiltonian into a spin-dependent part, \mathbf{B} , and a spin-independent component, H , yields that \mathcal{U} operates only on the spin-dependent part,

$$\mathcal{H}' = H + \mathbf{B} \cdot \mathcal{U}\boldsymbol{\sigma}\mathcal{U}^\dagger. \quad (3)$$

From the transformed Hamiltonians, \mathcal{H}' , the LDOS for the different directions can then be calculated using the regular recursion method and the magnetic density along the three directions can be obtained. From the three orthogonal directions, the local magnetization axis is calculated and the LDOS for the local spin axis can be constructed by taking the scalar product of the generalized magnetic density of states and the local magnetization vector. As all Hamiltonians are constructed within an *ab initio* LMTO-ASA formalism, all calculations are fully self-consistent, and the spin densities are treated within the local spin density approximation³⁶. Since the recursion procedure is performed for three orthogonal directions, the computational cost for each iteration is tripled compared with the collinear implementation of the RS-LMTO-ASA, but the linear scaling with respect to the number of nonequivalent atoms is retained.

The calculations of the transition metal clusters have been performed by embedding the clusters as a perturbation on a self-consistently converged perfect Cu(111) surface. The Cu surface has been calculated using the experimental lattice parameter of Cu. As is usually the case for LMTO-ASA methods, the vacuum outside the surface needs to be simulated by having a number of layers of empty spheres above the Cu surface in order to provide a basis for the wave-function in the vacuum and to treat charge transfers correctly. After embedding the cluster

on the surface, the charge and magnetization densities of the cluster atoms and the neighboring Cu atoms and empty spheres are then recalculated until self-consistency is obtained while the electronic structure for atoms far from the cluster are kept unchanged to their unperturbed values. Structural relaxations have not been included in this study, so the cluster sites have been placed on the regular fcc lattice above the Cu surface. Earlier studies on supported transition metal clusters⁴³ have shown that structural relaxations can change the magnetic properties of the clusters. On the other hand, in an experimental situation, small clusters as those considered in this study are usually constructed in an out-of-equilibrium situation by manipulation with an STM tip and calculated equilibrium geometries might therefore not be relevant. The most relevant relaxation for these kind of artificially created clusters would be the distance between the cluster atoms and the substrate atoms and since a noble metal substrate is used in this study, the interaction between clusters and substrate play a lesser role compared to the interactions between the cluster atoms. The clean Cu(111) surface has been modeled by a large (>5000) slab of atoms and the continued fraction, that occurs in the recursion method, have been terminated with the Beer-Pettifor⁴⁴ terminator after 30 recursion levels.

The non-collinear calculations have been performed without including the spin-orbit coupling. Since this term is neglected, a preferred spin axis does not exist in the system and the magnetic structures are thus only converged with respect to the directions of the magnetic moments relative to the other spin moments in the cluster. In order to minimize the risk of finding magnetic orderings that correspond to only a local minimum, several starting guesses were used for each system.

The calculated magnetic structures can be analyzed in terms of the exchange interactions J_{ij} between spins on atoms situated at sites i and site j . A well known connection between the exchange interactions and the magnetic ordering is given by the classical Heisenberg Hamiltonian,

$$\mathcal{H}_H = - \sum_{i,j,i \neq j} J_{ij} \cos\theta_{ij}, \quad (4)$$

where θ_{ij} is the angle between the magnetic moment on site i and site j . Note that in Eqn. 4, the magnitude of the spins have been incorporated into the effective J_{ij} interactions.

In this work, we have calculated exchange interactions directly using the Liechtenstein formula⁴⁵ as implemented in the RS-LMTO-ASA⁴⁶ for a large selection of the considered clusters. The J_{ij} 's shown in this study, have been obtained from the ferromagnetic configuration of the clusters. Other magnetic configurations typically result in different values of the J_{ij} 's, although the signs are seldom changed.⁴⁷ If the exchange interactions would be independent of θ_{ij} , the magnetic structure could in principle be calculated by minimizing the Heisenberg Hamiltonian with J_{ij} 's calculated from a ferromagnetic

configuration. This is not the case for the systems considered in this work, which motivates a full non-collinear calculation of the magnetic structures. However, on a qualitative level the cause of the magnetic ordering, e.g. the effect of frustration or the competition between nearest and next-nearest interactions, can still be discussed in terms of the calculated exchange interactions.

For a selection of Cr clusters, which are discussed in Sec. III C, our calculated magnetic structures has been compared to the structure found by minimizing the Heisenberg Hamiltonian for a fixed configuration of J_{ij} 's, where only nearest-neighbour interactions are finite. The minimization of the Heisenberg Hamiltonian for these clusters has been performed by a genetic search algorithm⁴⁸.

III. RESULTS

A. Fe clusters

In Fig. 1 the magnetic structure of several Fe clusters are shown. Regardless of the geometry of the studied Fe clusters, we find the magnetic ordering in the clusters to always be ferromagnetic. The collinear magnetic structure for these clusters, which can be put in contrast with the non-collinear ordering found for fcc structured Fe clusters embedded in bulk Cu⁴, could be caused by the fact that the decreased coordination of the surface clusters lead to a high-spin state which favours ferromagnetic coupling between neighbouring Fe atoms⁴⁹. This is also consistent with an analysis by Lizarraga *et al.*⁵⁰. It should be pointed out here that large magnetic moments do not automatically lead to collinear magnetism. As we will see in the section below, Mn is an example where large moments result in an antiferromagnetic interatomic exchange coupling, which on a frustrated geometry lead to non-collinear magnetism. In the case of Fe the large calculations result in large moments and a ferromagnetic interatomic exchange coupling.

The spin moments for the Fe atoms in the clusters shown in Fig. 1 range between 3.45 μ_B for the atoms in the dimer to 2.56 μ_B for the central atom in the seven atom cluster displayed in Fig. 1(d). It has been shown for Co clusters in Cu(001)³⁵ and Fe clusters on Ni and Cu surfaces⁵¹, that the magnetic moment has a linear behavior as function of the number of cluster neighbors around the site. The spin moments of the Fe clusters on Cu(111) of Fig. 1 show a similar trend and depend almost linearly on the number of nearest Fe neighbours. For these ferromagnetic Fe clusters, the orbital moments were calculated and they were also found to depend on the number of nearest neighbours. The largest orbital moment was found to be 0.15 μ_B per atom for the atoms in the dimer, and the smallest orbital moment is 0.06 μ_B for the central atom in the cluster shown in Fig. 1(d).

Due to the strong correlation between the magnetic moment for the atoms in the Fe clusters and the num-

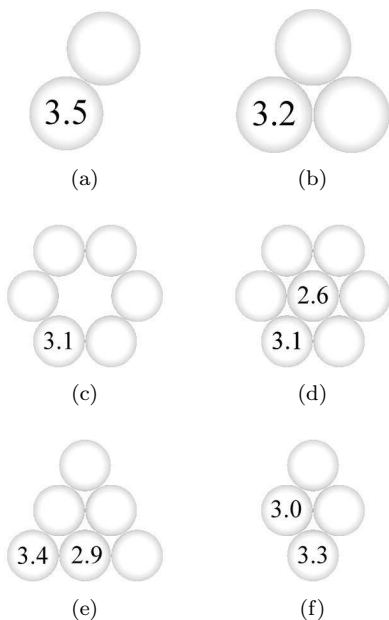


FIG. 1: The geometries for clusters of Fe atoms on a Cu(111) surface. All Fe clusters are found to exhibit a ferromagnetic ground state regardless of the cluster structure. The numbers indicate the atom projected spin moment of the different atoms.

ber of Fe neighbours, the magnetic moments obtained above can in principle be used to predict the total magnetic moment of any Fe cluster as long as the shape is determined and the cluster is planar. This would indicate that the magnetic moment per atom for a perfect monolayer of Fe atoms on a Cu(111) surface would be $\sim 2.7 \mu_B$ which is in good agreement with earlier calculations of Fe monolayers on Cu^{52,53,54,55}. Our findings of ferromagnetic coupling indicate that a single Fe monolayer would be ferromagnetic in agreement with Ref. 52 whereas Ref. 53 found that a single row antiferromagnetic order would be the most stable magnetic configuration. This discrepancy may be explained by the use of different lattice parameters in Refs. 52 and 53.

B. Mn clusters

In a previous paper³¹ we showed that due to antiferromagnetic coupling between nearest neighbour atoms in Mn clusters deposited on Cu one finds either a collinear antiferromagnetic structure or, if frustration occurs due to the cluster geometry, a non-collinear magnetic structure. A collection of frustrated cluster geometries with triangular shapes is shown in Fig. 2. The magnetic moments obtained for each atom of the studied Mn cluster are shown in Table. I. For the equilateral triangle in Fig. 2(a) a non-collinear arrangement with angle of 120° between the magnetic moments is the most stable configuration. The total energy difference between the stable

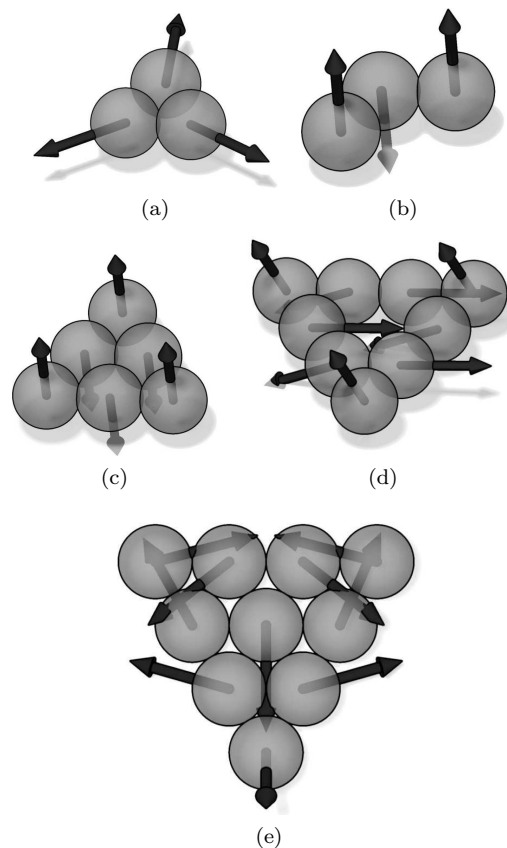


FIG. 2: The calculated magnetic ordering for triangular Mn clusters on a Cu(111) surface. For all geometries except the isosceles triangle shown in (b) and the six atom triangle in (c), non-collinear solutions are obtained due to magnetic frustration.

non-collinear solution and a frustrated collinear antiferromagnetic solution, with two spins parallel to each other and anti-parallel to the third spin is 13 meV/atom. The ferromagnetic solution was found to have an energy of 102 meV/atom higher than the stable non-collinear solution. The isosceles triangle shown in Fig. 2(b) has an antiferromagnetic collinear ground state which indicates that the exchange coupling between the two Mn atoms furthest from each other is either very small compared to the antiferromagnetic nearest-neighbour exchange coupling or has the opposite sign (i.e. ferromagnetic). As the size of the triangular clusters increases (Figs. 2(c) to 2(e)), the behaviour becomes more intricate. Although the six-atom triangle (Fig. 2(c)) by the analogous geometry as the three atom triangle in Fig. 2(a), could be expected to align in a structure with 120° between neighbouring atoms, it is in fact a collinear antiferromagnetic order that is the most stable solution. The energy difference between the collinear structure and a non-collinear structure was found to be 18 meV/atom. The cause for the preferred collinear order is the different environment for the corner atoms who only have two nearest neigh-

bours compared to the three central atoms who have four nearest neighbours each. The reduced coordination for the corner atoms causes their antiferromagnetic exchange coupling to nearest neighbours to be enhanced. The calculated J_{ij} s confirm this behaviour since the strength of the exchange interaction between a corner atom and a nearest-neighbour amounts to -27 meV while it is -12 meV between two central atoms. A similar mechanism can be expected for the nine-atom cluster displayed in Fig. 2(d), but for this geometry the atoms that are not situated at the corners of the triangle have three nearest neighbours due to the hole in the middle of the cluster. Therefore the difference in the local geometry is smaller between the corner atoms and the central atoms which leads to a more delicate balance of the exchange couplings. The resulting structure has the moments pointing in three different directions instead of two directions which would be the case for a collinear antiferromagnetic solution. The angle between two neighbouring central atoms is 152° while the angle between a corner atom and a nearest-neighbour is 104° . Contrary to what was found for the six atom cluster in Fig. 2(c), it thus appears that the exchange coupling is larger between central atoms than between a corner atom and a central atom. This behaviour is supported by the calculated J_{ij} s where the coupling between an corner atom and a nearest-neighbour is -9meV while the exchange coupling is found to be -36 meV between two central atoms. The non-collinear solution for the nine atom cluster has a total energy which is 13me V/atom lower than a collinear antiferromagnetic solution.

The analysis of the final ten-atom triangle shown in Fig. 2(e) is even more complicated. From a geometrical view, this cluster has three nonequivalent sites; the three corner atoms, the six atoms neighbouring to the corner atoms and the central atom. The magnetic structure does however have a lower symmetry that can be described by decomposing the cluster into the central atom and three 'sub-triangles', consisting of the three atoms closest to each corner of the cluster. Within each sub-triangle, the three atoms couple to each other in a geometry that resembles the 120° structure of a single three atom triangular cluster, but since exchange interactions from other neighbouring atoms are present as well, the angles between the moments in these sub-triangles vary between 146° and 104° . All angles between the moments for the atoms in the ten atom cluster can be seen in Table II. The influence of the different number of neighbours for the cluster atoms determine their magnetic moments where the corner atoms have a magnetic moment of $4.3 \mu_B$, the central atom has $2.6 \mu_B$ and the magnetic moment for the remaining six atoms is $3.6 \mu_B$.

Atomic wires constitute a group of nanostructures that has attracted a lot of attention^{3,56,57}. We have calculated the magnetic structure for wires of Mn atoms with lengths between two to nine atoms. The wires are oriented along a $1\bar{1}0$ direction on the Cu surface. The total energy differences, per cluster atom, between the anti-

TABLE I: Magnetic moments (in μ_B) for atoms in the clusters displayed in Fig. 2(a)-2(e). The atoms are numbered in the left column, starting from the leftmost atom, increasing around the cluster in the clockwise direction and, for the largest cluster, ending with the central atom.

	2(a)	2(b)	2(c)	2(d)	2(e)
1	4.25	4.54	4.33	4.15	4.25
2	4.25	4.23	3.57	3.77	3.56
3	4.25	4.54	4.33	3.77	3.56
4	-	-	3.57	4.15	4.25
5	-	-	4.37	3.77	3.56
6	-	-	3.57	3.77	3.56
7	-	-	-	4.15	4.25
8	-	-	-	3.77	3.56
9	-	-	-	3.77	3.56
10	-	-	-	-	2.64

TABLE II: The magnetic configuration described by angles between moments for atoms in the cluster displayed in Fig. 2(e). The atoms are numbered starting from the leftmost atom, increasing around the cluster in the clockwise direction and ending with the central atom.

Atom	1	2	3	4	5	6	7	8	9	10
1	0	146	52	147	57	20	90	150	104	103
2	146	0	98	52	155	158	56	60	107	52
3	52	98	0	146	107	60	56	158	155	52
4	147	52	146	0	104	150	90	20	57	103
5	57	155	107	104	0	47	138	96	49	150
6	20	158	60	150	47	0	108	141	96	107
7	90	56	56	90	138	108	0	108	138	53
8	150	60	158	20	96	141	108	0	47	107
9	104	107	155	57	49	96	138	47	0	150
10	103	52	52	103	150	107	53	107	150	0

ferromagnetic and the ferromagnetic magnetic configurations for the Mn wires are shown in Fig. 3. A large energy difference of 96 meV/atom is found for the dimer whereas the energy differences for the longer wires are significantly smaller. If only nearest neighbour interactions played role one would expect an energy difference (per atom) between ferromagnetic and antiferromagnetic coupling with a functional form $J(1-\frac{1}{N})$, where N is the number of atoms in the wire. Hence for long chains this energy difference should be equal to J whereas the energy difference would continuously become smaller and reach the value J/2 for N=2. The data in Fig. 3 does not display this trend, which suggests that next-nearest neighbour interactions are important and/or that the value of J depends on the number of atoms of the cluster.

For the dimer and trimer only a collinear antiferromagnetic solution is found, whereas, for longer chains a slightly canted non-collinear order is also found. For almost all of the longer chains, the non-collinear solutions

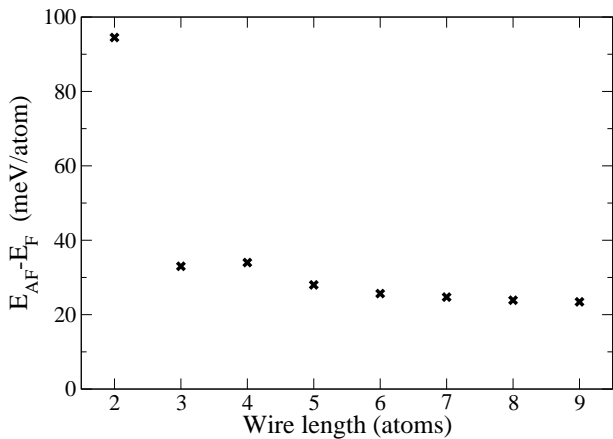


FIG. 3: Total energy differences between antiferromagnetic, E^{AF} , and ferromagnetic, E^{FM} , configurations of wires of Mn atoms, oriented along a $(1\bar{1}0)$ direction on a Cu(111) surface.

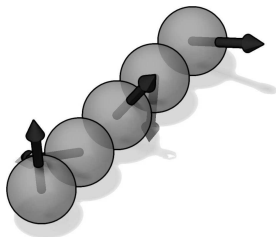


FIG. 4: Calculated magnetic configurations for a five atomic Mn wire, oriented along a $(1\bar{1}0)$ direction on a Cu(111) surface.

are unstable, but resembles the collinear antiferromagnetic solution closely, both in energy, in all cases less than 0.5 meV/atom, and in the angular difference, where the deviation from the collinear structure is smaller than 3° per atomic pair.

The Mn pentamer is however an interesting exception from the behavior of the other wires, and for this system, the ground state is actually found to be a non-collinear configuration, shown in Fig. 4. The non-collinear configuration for the pentamer can be described by the angle between an edge atom and its nearest neighbour, which is 170° , and the angle between two neighbouring central atoms, which is 155° . The energy difference between the non-collinear and the antiferromagnetic solutions for the pentamer is 2 meV/atom.

The straight wires does not have geometries that cause frustration in the same way as the triangular clusters mentioned earlier, so a probable cause for the non-collinearity of the Mn pentamer is the competition between ferromagnetic and antiferromagnetic exchange interactions between the different atoms in the cluster. Since the nearest-neighbour interactions are always antiferromagnetic for the Mn clusters (at least for the nearest-neighbour distance used in this study), more

TABLE III: Calculated exchange parameters J_{ij} (in meV) for the Mn pentamer shown in Fig. 4. The atoms are numbered from left to right.

$i \setminus j$	1	2	3	4	5
1	-	-34	-5.0	6.3	-3.6
2	-34	-	-12	-11	6.3
3	-5.0	-12	-	-12	-5.0
4	6.3	-11	-12	-	-34
5	-3.6	6.3	-5.0	-34	-

long-range interactions must play a role in destabilizing the collinear magnetic state. In order to examine the size and range of the exchange interactions, we have calculated exchange coupling parameters J_{ij} for the five atom wire shown in Fig. 4. The values of the exchange parameters are shown in Table III where the i and j are chosen so that site 1 and 5 are the edge atoms and site 3 is the central atom. Hence site 2 is nearest neighbour to site 1 and 3 and the nearest neighbours for site 4 is site 3 and 5. It may be observed that the exchange interactions are strongest and antiferromagnetic between nearest neighbours, with a smaller long range interaction that oscillates between ferromagnetic and antiferromagnetic coupling. The largest magnitude for the exchange interaction is obtained for J_{12} and J_{45} , i.e. between an edge atom and its nearest neighbour. Furthermore, Table III shows that although the nearest neighbour interactions have the largest magnitude, the more long ranged interactions always seem to counteract the nearest neighbour interactions. This might not be obvious from the values in Table III but as a clarifying example we can examine the exchange interactions between atom 1 and the other atoms. The negative nearest neighbour interactions in the pentamer would prefer an antiferromagnetic order so that atom 1 would be ferromagnetically coupled to atom 3 and atom 5, and antiferromagnetically coupled to atoms 2 and 4. However, the calculated exchange interactions in Table III show that the J_{13} and J_{15} are in fact negative while J_{14} is positive, thus competing against the antiferromagnetic nearest-neighbour ordering, which results in the non-collinear magnetic state shown in Fig. 4.

C. Cr clusters

In Fig. 5 the geometries and calculated magnetic configurations for a selection of Cr clusters are shown. Calculations for Mn clusters with similar geometries can be found elsewhere.³¹ The magnetic moments obtained for each atom of the Cr clusters shown in Fig. 5 can be seen in Table. IV. The magnetic structures are for most of the clusters quite similar to the calculated magnetic structure for Mn clusters although certain differences occur, as will be commented on below. Both the Cr dimer and a straight trimer (not shown) orders antiferromagnetically while a three atom triangle has the same non-collinear

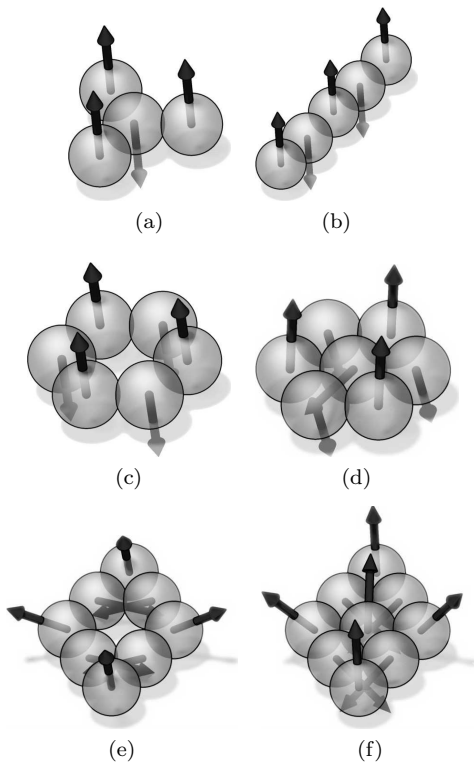


FIG. 5: The calculated magnetic ground state for Cr clusters on a Cu(111) surface.

TABLE IV: Magnetic moments (in μ_B) for atoms in the clusters displayed in Fig. 5(a)-5(f). The atoms are numbered starting from the leftmost atom, counting around the cluster in the clockwise direction and, if applicable, ending with the central atom.

	5(a)	5(b)	5(c)	5(d)	5(e)	5(f)
1	3.99	3.99	3.82	3.54	3.87	3.57
2	3.99	3.89	3.82	3.54	3.65	3.28
3	3.99	3.92	3.82	3.54	3.89	3.89
4	3.50	3.89	3.82	3.54	3.65	3.28
5	-	3.99	3.82	3.54	3.87	3.57
6	-	-	3.82	3.54	3.65	3.28
7	-	-	-	3.12	3.89	3.89
8	-	-	-	-	3.65	3.28
9	-	-	-	-	-	2.81

structure as its Mn counterpart, as shown in Fig. 2(a). It can be noted that this non-collinear structure has also been reported from calculations on Cr clusters, with the same geometry, supported on Au(111).^{58,59} The cluster in Fig. 5(a) has a collinear antiferromagnetic ground state since the edge atoms only have one nearest neighbour and therefore no frustration occurs. The pentamer in Fig. 5(b) also exhibits an antiferromagnetic ground-state, which in contrast to the non-collinear behaviour of the Mn pentamer, is purely collinear. This finding indicates

TABLE V: Calculated exchange parameters J_{ij} (in meV) for the Cr pentamer shown in Fig. 5(b). The atoms are numbered from left to right.

$i \setminus j$	1	2	3	4	5
1	-	-143	4.6	18.9	15.3
2	-143	-	-97.0	-40.5	18.9
3	4.6	-97.0	-	-97.0	4.6
4	18.9	-40.5	-97.0	-	-143
5	15.3	18.9	4.6	-143	-

that the magnetic structures of the Cr clusters are more strongly dependant on the nearest-neighbour exchange coupling than the Mn clusters are. The calculated exchange parameters J_{ij} for the Cr pentamer is shown in Table V. Compared with the exchange interactions for the Mn pentamer in Table III we see that the nearest-neighbour interactions are indeed larger between the Cr atoms. On the other hand, the more long ranged interactions also have larger magnitudes in the Cr pentamer than for the Mn counterpart. The exchange interactions between atoms further from each other do however not always compete against the nearest-neighbour interactions as was the case for the Mn pentamer.

The collinear antiferromagnetic behaviour found for the pentamer also occurs for the six atom ring displayed in Fig. 5(c), which is expected since the geometry does not cause frustration for the nearest-neighbour interactions. The cluster in Fig. 5(d) has a symmetric non-collinear ground state with an angle between two neighbouring atoms on the rim of the cluster of 157° and between the central atom and any outer atom the angle is 101° . This can be compared with the energy minimum obtained when minimizing the nearest-neighbour Heisenberg Hamiltonian where all nearest neighbour J_{ij} 's are set to be negative but equal. The Heisenberg model would give equilibrium angles of the same cluster geometry of between 151° outer neighbours and 104° between the central atom and any neighbour. Although the agreement between our calculated ground state and the Heisenberg minimum is good, it should be noted that due to the difference in the local structure around the central and outer atoms the exchange parameters J_{ij} should be different between two outer atoms compared to J_{ij} 's connecting to the central atom. This difference can be considered in a simple model analysis by damping the strength of the exchange parameters where the central atom is connected, and for a damping of 20% for these exchange parameters, the Heisenberg Hamiltonian approach yields an energy minimum with the angles of 157° for neighbouring outer atoms and 101° between the central atom and an edge atom which are in perfect agreement with our calculated angles.

Since the atoms of the hollow cluster in Fig. 5(e) do not all have only two nearest neighbours, as is the case for the other ring like geometry of Fig. 5(c), the cluster can not have an unfrustrated antiferromagnetic solution. De-

TABLE VI: Angles between magnetic moments for atoms in the cluster displayed in Fig. 5(e). The atoms are numbered starting from the leftmost atom and increasing along the clockwise direction of the cluster.

Atom	1	2	3	4	5	6	7	8
1	0	169	56	56	112	56	56	169
2	169	0	112	133	56	133	112	0
3	56	112	0	112	56	112	0	112
4	56	133	112	0	169	0	112	133
5	112	56	56	169	0	169	56	56
6	56	133	112	0	169	0	112	133
7	56	112	0	112	56	112	0	112
8	169	0	112	133	56	133	112	0

TABLE VII: Angles between magnetic moments for atoms in the cluster displayed in Fig. 5(f). The atoms are numbered starting from the leftmost atom, increasing along the clockwise direction of the cluster and ending with the central atom.

Atom	1	2	3	4	5	6	7	8	9
1	0	156	40	95	74	95	40	156	69
2	156	0	137	86	95	86	137	0	128
3	40	137	0	137	40	137	0	137	40
4	95	86	137	0	156	0	137	86	128
5	74	95	40	156	0	156	40	95	69
6	95	86	137	0	156	0	137	86	128
7	40	137	0	137	40	137	0	137	40
8	156	0	137	86	95	86	137	0	128
9	69	128	40	128	69	128	40	128	0

scribing the cluster with a Heisenberg Hamiltonian with equal and negative J_{ij} 's would yield a ground state with 120° between neighbouring atoms. As seen in Fig. 5(e) our calculated magnetic structure differs from the Heisenberg minimum, it is instead described with three different nearest-neighbour angles. The upper and lower edge atoms have an angle of 112° to their neighbours while the leftmost and rightmost of the atoms have an angle of 169° to their nearest neighbours. The third angle is that between two atoms with three neighbours each and they have an angle of 133° between them. This structure can be explained in a similar way as the cluster in Fig. 5(d) could, with different local geometries resulting in different strengths of the exchange coupling and thus different J_{ij} 's for different atoms. The angles between the different magnetic moments for the cluster shown in Fig. 5(e) are given in Table. VI.

Filling the empty site in the middle of the cluster in Fig. 5(e) gives the cluster geometry shown in Fig. 5(f). This additional atom causes the magnetic structure to be even more complex. Since the symmetry is lowered compared to the cluster in Fig. 5(d), the central atom does not have the same angle towards all of its neighbours. Instead two angles are needed to describe the

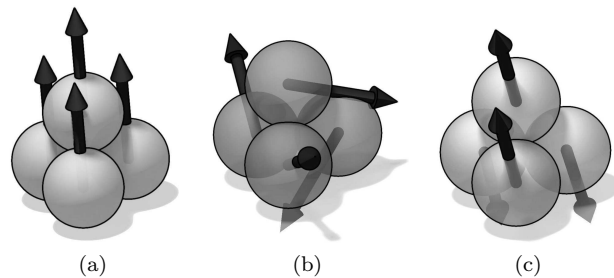


FIG. 6: The calculated magnetic ordering for pyramid shaped clusters on a Cu(111) surface. Fig. 6(a) shows a Fe cluster with a ferromagnetic solution. Fig. 6(b) shows a Mn cluster and Fig. 6(c) shows the Cr pyramid.

structure of the neighbours of the central atom. One of these is the angle of 69° which the central atom makes towards the leftmost and rightmost atoms and the other angle connects the central atom with the remaining four neighbours and the size of this angle is 128° . The upper and lower edge atoms makes an angle of 137° with their neighbours. The angles between different magnetic moments for the cluster shown in Fig. 5(f) are given in Table. VII.

D. Three dimensional clusters

So far the studied clusters have all been confined in one layer above the Cu surface. However, our method can treat three dimensional clusters as well. In order to demonstrate this we show the obtained magnetic configurations for a pyramid-like tetrahedron shaped cluster in Fig. 6. As expected from the results for Fe clusters reported earlier in this work, the Fe cluster (Fig. 6(a)) exhibits a ferromagnetic order. The atom situated on top of the pyramid has a magnetic moment of $3.40\mu_B$ while the three Fe atoms closer to the Cu surface have a magnetic moment of $3.11\mu_B$. For the Mn cluster shown in Fig. 6(b), a non-collinear structure is found and for the Cr pyramid, shown in Fig. 6(c) a collinear antiferromagnetic solution is found. A model Heisenberg Hamiltonian, as in Eqn. 4, with only antiferromagnetic nearest-neighbour exchange parameters, J_{ij} , of equal size, yields a two-fold degenerate ground state, either a collinear antiferromagnet or a non-collinear tetragonal configuration with 109° between neighbouring angles. The calculation for the Mn pyramid over Cu(111) shows angles which are slightly distorted relative to those of the free pyramid, around 116 degrees between the base atoms close to the substrate and angles of about 100 degrees between the base site and the top one. It is peculiar that the Mn cluster has the non-collinear tetragonal configuration as the ground state whereas the Cr cluster has the collinear antiferromagnetic ground state solution. A possible explanation for the non-collinear ground state of the Mn pyramid could be that, similar to the situation for several of the

planar clusters, the reduced neighbour coordination for the top atom compared to the atom in the base of the pyramid yields different exchange interaction strengths between the atoms in the cluster. The calculated exchange parameters confirm this since the exchange interaction between a top and a base atom is -83 meV while the interaction between two base atoms -46 meV. The reduced neighbour coordination also affects the magnetic moment for the top atom which is $4.5 \mu_B$ compared to $4.0 \mu_B$ for the base atoms. However, the situation with different exchange parameters is also present for the Cr pyramid where the interaction strength between the top atom and a base atom is -171 meV compared to -98 meV for the coupling between two base atoms. The magnetic moment for the Cr atom on top of the pyramid is $4.2 \mu_B$ while the magnetic moment for the base atoms is $3.6 \mu_B$. The difference in the magnetic ordering found for the Cr and Mn pyramids indicates that the bilinear exchange terms J cannot always describe the magnetic interactions between the atoms in supported magnetic clusters, a fact which previously been suggested for magnetic dimers on surfaces.⁶⁰ It can be noted that the difference in the total energy between the non-collinear ground state structure and the antiferromagnetic solution for the Mn cluster is 25 meV per atom while the corresponding difference for the Cr pyramid is -15 meV per atom.

IV. CONCLUSIONS

We have studied the magnetic structure of small clusters of Fe, Mn, and Cr supported on a Cu(111) surface with non-collinear, first principles calculations. The studied Fe clusters are found to order ferromagnetically

regardless of the cluster geometry. For Mn and Cr clusters, antiferromagnetic exchange interactions between nearest-neighbours are found to cause either collinear antiferromagnetic ordering or non-collinear ordering. The non-collinear ordering occurs when the cluster geometry is such that an antiferromagnetic arrangement becomes frustrated. The calculations have been accompanied by comparisons with calculated effective exchange interactions as well as with ground states obtained from a simplified Heisenberg Hamiltonian and the comparisons show that the exchange interactions vary for different atoms in the clusters as a result of the different local structure. Differences between the magnetic ordering for Mn and Cr clusters are found where Cr clusters seem to prefer collinear solutions to a higher degree while Mn clusters can exhibit non-collinear configurations even for unfrustrated cluster geometries. Comparisons with model Hamiltonians show that the magnetic structure of certain clusters can be explained by a simple nearest-neighbour Heisenberg Hamiltonian while other cluster geometries cause more complex behaviours.

V. ACKNOWLEDGEMENTS

We acknowledge financial support from the Göran Gustafsson foundation, the Swedish Research Council, the Swedish Foundation for Strategic Research, Lennanders Stiftelse, and CNPq, Brazil. The calculations were performed at the high performance computing centers UPPMAX, and PDC within the Swedish National Infrastructure for Computing and at the computational facilities of the LCCA, University of São Paulo and of the CENAPAD at University of Campinas, SP, Brazil.

* Current address: Département de Recherche Fondamentale sur la Matière Condensée, SP2M/LSim, CEA-Grenoble, 38054 Grenoble Cedex 9, France

† Electronic address: Olle.Eriksson@fysik.uu.se

¹ G. Binnig and H. Rohrer, *Helv. Phys. Acta.* **55**, 726 (1982).

² F. J. Himpsel, J. E. Ortega, G. J. Mankey, and R. F. Willis, *Adv. Phys.* **47**, 511 (1998).

³ P. Gambardella, M. Blanc, K. Kuhnke, K. Kern, F. Picaud, C. Ramseyer, C. Girardet, C. Barreateau, D. Spanjaard, and M. C. Desjonquères, *Phys. Rev. B* **64**, 045404 (2001).

⁴ Y. Tsunoda, *Journal of Physics: Condensed Matter* **1**, 10427 (1989).

⁵ E. Sjöstedt and L. Nordström, *Phys. Rev. B* **66**, 014447 (2002).

⁶ E. Fawcett, *Rev. Mod. Phys.* **60**, 209 (1988).

⁷ P. Bodeker, A. Schreyer, and H. Zabel, *Phys. Rev. B* **59**, 9408 (1999).

⁸ R. Robles, E. Martinez, D. Stoeffler, and A. Vega, *Phys. Rev. B* **68**, 094413 (2003).

⁹ A. Bradley and J. Thewlis, *Proc. R. Soc. London* **115**, 465 (1927).

¹⁰ D. Hobbs, J. Hafner, and D. Spisak, *Phys. Rev. B* **68**,

014407 (2003).

¹¹ T. Eriksson, R. Lizarraga, S. Felton, L. Bergqvist, Y. Andersson, P. Nordblad, and O. Eriksson, *Phys. Rev. B* **69**, 054422 (2004).

¹² T. Eriksson, L. Bergqvist, Y. Andersson, P. Nordblad, and O. Eriksson, *Phys. Rev. B* **72**, 144427 (2005).

¹³ I. M. L. Billas, J. A. Becker, A. Chatelain, and W. A. de Heer, *Phys. Rev. Lett.* **71**, 4067 (1993).

¹⁴ M. B. Knickelein, *Phys. Rev. Lett.* **86**, 5255 (2001).

¹⁵ D. C. Douglass, J. P. Bucher, and L. A. Bloomfield, *Phys. Rev. B* **45**, 6341 (1992).

¹⁶ C. Kohl and G. F. Bertsch, *Phys. Rev. B* **60**, 4205 (1999).

¹⁷ T. Morisato, S. N. Khanna, and Y. Kawazoe, *Phys. Rev. B* **72**, 014435 (2005).

¹⁸ R. C. Longo, E. G. Noya, and L. J. Gallego, *Phys. Rev. B* **72**, 174409 (2005).

¹⁹ J. T. Lau, A. Föhlisch, R. Nietubyc, M. Reif, and W. Wurth, *Phys. Rev. Lett.* **89**, 057201 (2002).

²⁰ C. Binns, K. W. Edmonds, S. H. Baker, S. C. Thornton, and M. D. Upward, *Scripta Mater.* **44**, 1303 (2001).

²¹ D. Spisak and J. Hafner, *Phys. Rev. B* **65**, 235405 (2002).

²² B. Lazarovits, L. Szunyogh, P. Weinberger, and B. Uj-

- falussy, Phys. Rev. B **68**, 024433 (2003).
- ²³ V. S. Stepanyuk, W. Hergert, P. Rennert, K. Wildberger, R. Zeller, and P. H. Dederichs, J. Magn. Magn. Matter **165**, 272 (1997).
- ²⁴ V. S. Stepanyuk, W. Hergert, K. Wildberger, S. K. Nayak, and P. Jena, Surf. Sci. **384**, L892 (1997).
- ²⁵ V. S. Stepanyuk, W. Hergert, P. Rennert, K. Kokko, A. F. Tatarchenko, and K. Wildberger, Phys. Rev. B **57**, 15585 (1998).
- ²⁶ V. U. S. Uzdin and C. Demangeat, Europhys. Lett. **47**, 556 (1999).
- ²⁷ V. U. S. Uzdin and C. Demangeat, Surf. Sci. **482**, 965 (2001).
- ²⁸ S. Lounis, P. Mavropoulos, P. H. Dederichs, and S. Blügel, Phys. Rev. B **72**, 224437 (2005).
- ²⁹ R. Robles and L. Nordström, Phys. Rev. B **74**, 094403 (2006).
- ³⁰ S. Lounis, M. Reif, P. Mavropoulos, L. Glaser, P. H. Dederichs, M. Martins, S. Blügel, and W. Wurth, condmat/0608048.
- ³¹ A. Bergman, L. Nordström, A. B. Klautau, S. Frota-Pessôa, and O. Eriksson, Phys. Rev. B **73**, 174434 (2006).
- ³² O. K. Andersen, Phys. Rev. B **12**, 3060 (1975).
- ³³ R. Haydock, *Solid State Physics* (Academic, New York, 1980), vol. 35, p. 216.
- ³⁴ S. Frota-Pessôa, Phys. Rev. B **46**, 14570 (1992).
- ³⁵ A. Klautau and S. Frota-Pessôa, Surf. Sci. **579**, 27 (2005).
- ³⁶ V. von Barth and L. Hedin, J. Phys. Chem. **5**, 1629 (1972).
- ³⁷ J. Kübler, K.-H. Höck, J. Sticht, and A. R. Williams, J. Phys. F **18**, 469 (1988).
- ³⁸ L. M. Sandratskii and P. G. Guletskii, J. Phys. F **16**, L43 (1986).
- ³⁹ L. Nordström and D. J. Singh, Phys. Rev. Lett. **76**, 4420 (1996).
- ⁴⁰ L. Sandratskii, Adv. Phys. **91**, 47 (1998).
- ⁴¹ H. M. Petrilli and S. Frota-Pessôa, J. Phys. Condens. Matter **2**, 135 (1990).
- ⁴² K. K. Saha and A. Mookerjee, J. Phys. Condens. Matter **17**, 287 (2005).
- ⁴³ S. Pick, V. S. Stepanyuk, A. N. Baranov, W. Hergert, and P. Bruno, Phys. Rev. B **68**, 104410 (2003).
- ⁴⁴ N. Beer and D. Pettifor, *The Electronic Structure of Complex Systems* (Plenum Press, New York, 1984).
- ⁴⁵ A. I. Liechtenstein, M. I. Katsnelson, V. P. Antropov, and V. A. Gubanov, J. Magn. Magn. Matter **67**, 65 (1987).
- ⁴⁶ S. Frota-Pessôa, R. B. Muniz, and J. Kudrnovsky, Phys. Rev. B **62**, 5293 (2000).
- ⁴⁷ S. Frota-Pessôa and A. Klautau, Int. J. Mod. Phys. B **20**, 5281 (2006).
- ⁴⁸ I. G. Tsoulos and I. E. Lagaris, Comp. Phys. Comm. **174**, 152 (2006).
- ⁴⁹ B. Ujfalussy, L. Szunyogh, and P. Weinberger, Phys. Rev. B **54**, 9883 (1996).
- ⁵⁰ R. Lizarraga, L. Nordström, L. Bergqvist, A. Bergman, E. Sjöstedt, P. Mohn, and O. Eriksson, Phys. Rev. Lett. **93**, 107205 (2004).
- ⁵¹ R. Z. P. Mavropoulos, S. Lounis and S. Blügel, Appl. Phys. A **82**, 103 (2006).
- ⁵² P. Krüger, M. Taguchi, and S. Meza-Aguilar, Phys. Rev. B **61**, 15277 (2000).
- ⁵³ D. Spisak and J. Hafner, Phys. Rev. B **67**, 134434 (2003).
- ⁵⁴ O. Hjortstam, J. Trygg, J. M. Wills, B. Johansson, and O. Eriksson, Phys. Rev. B **53**, 9204 (1996).
- ⁵⁵ G. W. Fernando and B. R. Cooper, Phys. Rev. B **38**, 3016 (1988).
- ⁵⁶ B. Ujfalussy, B. Lazarovits, L. Szunyogh, G. M. Stocks, and P. Weinberger, Phys. Rev. B **70**, 100404(R) (2004).
- ⁵⁷ H. J. Lee, W. Ho, and M. Persson, Phys. Rev. Lett. **92**, 186802 (2004).
- ⁵⁸ H. J. Gotsis, N. Kioussis, and D. A. Papaconstantopoulos, Phys. Rev. B **73**, 014436 (2006).
- ⁵⁹ A. Bergman, L. Nordström, A. Klautau, S. Frota-Pessôa, and O. Eriksson, J. Phys. Condens. Matter **19**, 156226 (2007).
- ⁶⁰ A. T. Costa, R. B. Muniz, and D. L. Mills, Phys. Rev. Lett. **94**, 137203 (2005).